IEEE Photonics Journal
An IEEE Photonics Society Publication

Open Access

Deuterated SiN/SiON Waveguides on Si Platform and Their Application to C-Band WDM Filters

Volume 9, Number 5, October 2017

Tatsurou Hiraki
Takuma Aihara
Hidetaka Nishi
Tai Tsuchizawa

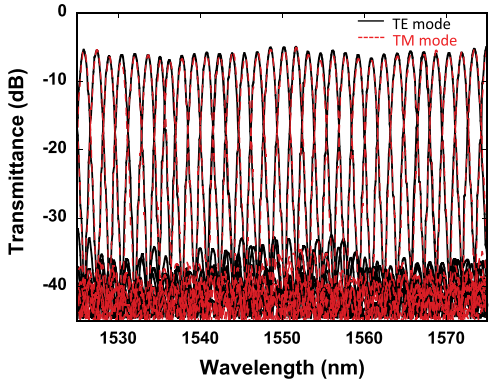

DOI: 10.1109/JPHOT.2017.2731996
1943-0655

Deuterated SiN/SiON Waveguides on Si Platform and Their Application to C-Band WDM Filters

Tatsurou Hiraki, Takuma Aihara, Hidetaka Nishi, and Tai Tsuchizawa

NTT Device Technology Labs, NTT Corporation, Kanagawa 243-0198, Japan.

DOI:10.1109/JPHOT.2017.2731996

Manuscript received June 19, 2017; revised July 18, 2017; accepted July 21, 2017. Date of publication July 29, 2017; date of current version August 14, 2017. Corresponding author: Tatsurou Hiraki (e-mail: hiraki.tatsurou@lab.ntt.co.jp).

Abstract: We describe low-loss SiN/SiON waveguides for wavelength-division-multiplexing filters on a Si platform. The key technology is a low-temperature deposition of refractive-index-controllable SiN/SiON films by using a hydrogen-free gas source (SiD_4), which avoids the strong optical absorption due to N-H bond. Using this technology, we demonstrate a low-loss ring resonator with a SiN waveguide, whose loss is 0.47 dB/cm at 1550 nm. It shows excess loss of 2.7 dB, a 3-dB bandwidth of 0.13 nm, and an extinction ratio of 27 dB in the entire C band. In addition, we also demonstrate a polarization-insensitive arrayed-waveguide grating with a SiON waveguide, whose loss is 0.29 dB/cm at 1550 nm. It shows insertion loss of 5.3 dB, crosstalk of less than −27 dB, and polarization insensitivity in the entire C band.

Index Terms: Silicon nanophotonics, waveguide devices.

1. Introduction

With the rapidly increasing demand for cost-effective wavelength-division-multiplexing (WDM) systems, silicon (Si) photonics platforms are attracting attention for the integration of optical devices, such as modulators, photodetectors, and wavelength filters [1]–[6]. In next generation telecommunications networks with advanced modulation [7]–[9], wavelength filters are key components for meeting the severe system requirements, including low loss, low interchannel crosstalk, polarization insensitivity, and high acceptable power. However, conventional Si wavelength filters have difficulty meeting these requirements due to the following issues. One is that their effective refractive indices are considerably varied by fabrication errors. For example, in fabricating a 200-GHz-grid arrayed-waveguide grating (AWG) with crosstalk of less than −20 dB, the allowable fabrication error for Si-waveguide AWG is on an angstrom order [10], [11], which cannot be achieved even if we use state-of-the-art fabrication technology. The other issue is the nonlinear optical effect. The nonlinear optical coefficient of Si waveguides is over ten times larger than that of commercialized silica-based waveguides. Therefore, the acceptable power and crosstalk reduction are limited by two-photon absorption and four-wave mixing [12].

A reasonable solution is to use alternative waveguide materials, such as Si-rich silicon nitride, silicon nitride and silicon oxynitride (SiN/SiON) [13], [14]. Their wide-range and medium index contrasts (3∼20%) enable us to balance the fabrication tolerance and the size reduction. In addition, their nonlinear coefficients are typically over ten times smaller than that of Si, which is useful in

reducing the nonlinear effects and increasing the acceptable power. In the previous work, SiN/SiON waveguides have been constructed on a Si photonics platform. For example, SiN waveguides with an index contrast of ∼20% have been used to construct AWGs [15], [16] and ring filters [17], [18]. In addition, for polarization insensitivity in a wavelength filter, a SiON waveguide with a much lower index contrast (∼3%) has been used in an AWG [19].

Although SiN/SiON waveguides have various advantages, there is an issue to use them for practical WDM applications [7]–[9]. The essential problem is how to fabricate them in the back-end-on-line (BEOL) process on a Si platform to prevent thermal damage to the active devices. Typically, they have been formed by the plasma-enhanced chemical vapor deposition (PECVD) method at temperatures less than ∼350 degrees Celsius. However, the gas source for the PECVD, such as silane (SiH_4), generates hydrogen atoms and forms N-H bonds, which have a large optical absorption coefficient at a wavelength of 1500 nm. The residual N-H bonds in the films make it difficult to apply them to low-loss WDM filters in the C band. Although the N-H bonds can be removed by post-deposition annealing, the required temperature is over 1000 degrees, which far exceeds the allowable temperature of the BEOL process. In this paper, we report a low-loss SiN/SiON waveguide, fabricated at less than 300 degrees Celsius. The key feature of the fabrication is the use of a hydrogen-free gas source for the deposition of the SiON film. Using the technology, we demonstrate a low-loss SiN-waveguide ring resonator and a polarization-insensitive SiN/SiON-waveguide AWG in the entire C band.

2. Hydrogen-Free SiN/SiON Film Formation

The key feature of the technology is the use of a hydrogen-free gas source for the PE CVD to avoid N-H bond formations. A promising gas source is a deuterated silane (SiD_4) [20]. The atomic mass of deuterium (D) is larger than that of hydrogen; therefore, the absorption peak wavelength due to N-D bonds is far from the telecommunications wavelength region. With SiD_4 gas, we can control the refractive index of SiON/SiN films by changing the gas-flow ratio in the electron-cyclotron-resonance (ECR) PECVD process. The ECR PECVD is preferable for controlling refractive indices at low temperature because the ECR plasma easily dissociates gas molecules [21], [22]. Fig. 1(a) shows the relationships between the refractive index and the gas-flow ratio of $N_2/(N_2 + O_2)$ at 200 degrees Celsius. The gas flow rates of SiD_4, Ar, and $N_2 + O_2$ were 40, 10, and 100 standard cubic centimeters per minute (sccm), respectively. The measured results indicate that the refractive indices gradually increase (ranging from 1.47 to 1.87) when the N_2 flow rate is increased. Fig. 1(a) also shows the relationships between the deposition rate and gas-flow ratio. The deposition rates (90 ∼ 100 nm/min) were reasonable for nanometer-order thickness control. The rate can be controlled by adjusting the SiD_4 flow rate and microwave power of the ECR plasma.

To evaluate the atomic composition of the deposited films, we used hydrogen forward scattering spectrometry (HFS) to detect the hydrogen and deuterium atoms. The measured samples were 100-nm-thick films with refractive indices of 1.515 and 1.87. Fig. 1(b) and (c) show the HFS spectrum. In the measurements, the incident ions and energy were $^4He^{++}$ and 2300 keV, the incident angle was 75 degrees, and the recoil angle was 30 degrees. Both films exhibit two peaks corresponding to the difference in the atomic mass. By fitting the theoretical curves, we found that the energies of the large and small peaks were corresponding to those of the deuterium and the hydrogen atoms, respectively. These results indicate that deuterium atoms were mainly introduced into the film during the ECR CVD process. The residual hydrogen would come from the ECR CVD chamber, and it can be prevented by using well-conditioned CVD equipment. To quantify the atomic percentages of all the atoms, we also used Rutherford backscattering spectrometry (RBS) [22]. Table 1 summarizes the estimated atomic percentages of all atoms in the films deposited by the SiD_4 gas (SiON:D, SiN:D). As a reference, it also shows the atomic percentages of the traditional films deposited by using an SiH_4 gas source (SiON:H, SiN:H). The estimated atomic compositions are $SiO_{1.75}N_{0.28}$:$D_{0.18}$ and $SiN_{1.50}$:$D_{0.67}$ for indices of 1.515 and 1.87, respectively. The refractive indices were mainly determined by the atomic-composition ratio of the oxygen and nitrogen, and this is consistent with the relationships between the refractive index and gas-flow ratio [see Fig. 1(a)].

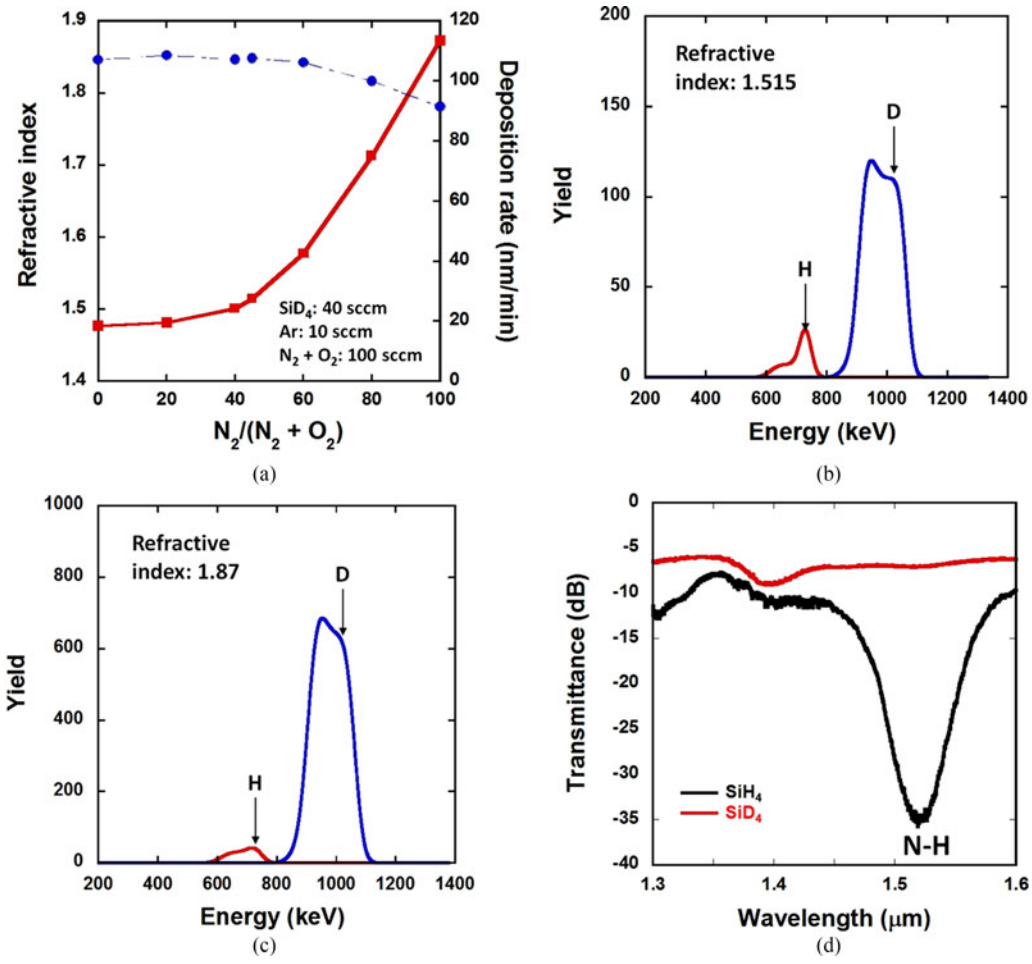

Fig. 1. (a) Relationship between refractive indices and deposition rate and gas-flow ratios. HFS spectrum of SiON/SiN films with refractive indices of (b) 1.515 and (c) 1.87. (d) Transmission spectrum of SiN:D and SiN:H waveguides using a core with the refractive indices of 1.87.

Notably, the atomic percentages of the residual hydrogen in the SiON:D/SiN:D film was over ten times lower than that in the traditional films. The results clearly show the SiD_4 gas source is useful for reducing hydrogen dissociation.

To examine the transparency of the films, we fabricated waveguides using the refractive index of 1.87 with the SiN:D film and the conventional SiN:H film, and compared their transparency. Fig. 1(d) shows the transmission spectrum of 1.8-cm-long waveguides fabricated by using the SiN:D and SiN:H films. The absorption peak at a wavelength of around 1500 nm is clearly reduced by using the SiD_4 gas. These results indicate the N-H bonds were successfully reduced by using the hydrogen-free gas source. Here, the residual O-H bond peak at around 1350 nm would be caused by the SiO_2 overcladding. We believe it can be also eliminated by using SiO_2:D for the overcladding film in the same process scheme.

3. SiN:D/SiON:D Waveguides and Their Applications

3.1 Characteristics of SiN:D Waveguide and Ring Filter

We used the SiN:D waveguide to construct a ring resonator on a Si substrate. The ring filter round-trip length was 324 μm, and the designed free spectral range (FSR) was 3.9 nm. The fabrication process was as follows. First, a 0.55-μm-thick SiN:D film was deposited on a 3-μm-thick SiO_2

TABLE 1
Atomic Percentages

Sample	Refractive index	Si (%)	O (%)	N (%)	H (%)	D (%)	Ar (%)
SiON:D	1.515	31.1	54.2	8.7	0.3	5.6	0.1
SiN:D	1.873	31.1	-	46.7	1.2	20.9	0.1
Ref. SiON:H	1.515	32.0	59.0	4.9	3.9	-	0.1
Ref. SiN:H	1.890	32.3	-	47.0	20.6	-	0.1

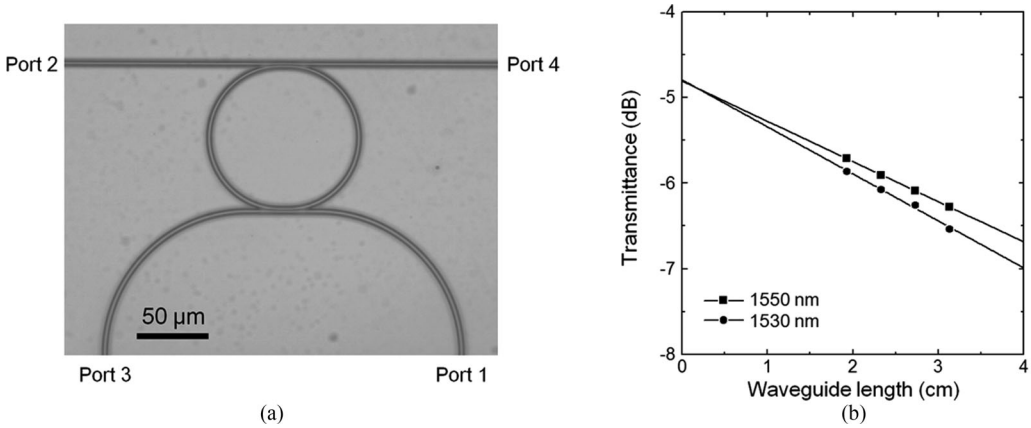

Fig. 2. (a) Microscope image of fabricated ring filter and (b) transmission characteristics of waveguide at wavelengths of 1530 and 1550 nm.

undercladding film on a Si substrate. Afterwards, the SiN:D film was patterned using electron-beam lithography and reactive-ion etching to form SiN:D waveguide cores with a width of 1.1 μm. Finally, the SiO_2 overcladding was deposited on the patterned SiN:D waveguide cores using PECVD with a tetraethoxysilane source. Fig. 2(a) shows a microscope photograph of the fabricated ring filter. All process temperatures were compatible with the BEOL temperature. First, we measured the propagation loss of the fabricated 0.55 $\times$ 1.1 μm^2 SiN:D waveguide in the C band. At the input and output facets, the SiN core width was widened to 3 μm by a 300-μm-long linear taper. The transverse electric (TE) mode light was coupled to the SiN:D waveguide through a lensed optical fiber. Fig. 2(b) shows the measured transmittances at wavelengths of 1530 and 1550 nm. The transmittance was normalized by the fiber-to-fiber transmittance. The propagation losses from the linear approximation were 0.55 and 0.47dB/cm at 1530 and 1550 nm, respectively. At 1530 nm near the absorption peak due to the N-H bonds, the measured loss was comparable to that at 1550 nm, and far smaller than that of the conventional SiN:H waveguide. This indicates that the N-H bonds in the SiN core were successfully removed with the BEOL process. Afterwards, we measured the transmission spectra of the fabricated ring filter from port 1 to 4 (drop port) and from port 2 to 4 (through port). Fig. 3(a) shows the measured transmission spectra in the C band. The transmission spectra were normalized by the fiber-to-fiber transmittance. Owing to the low-loss SiN:D waveguide, the performance of the SiN ring resonator was not degraded in the entire C bands. Fig. 3(b) shows the transmission spectra normalized by the transmittance of the reference SiN:D waveguide, whose length was 1.1 cm. The excess loss of port 1 to 4 was 2.7 dB, corresponding to the micro-ring loss of only 0.1 dB. The measured FSR was 3.9 nm for both from port 1 to 4 and from port 2 to 4. These

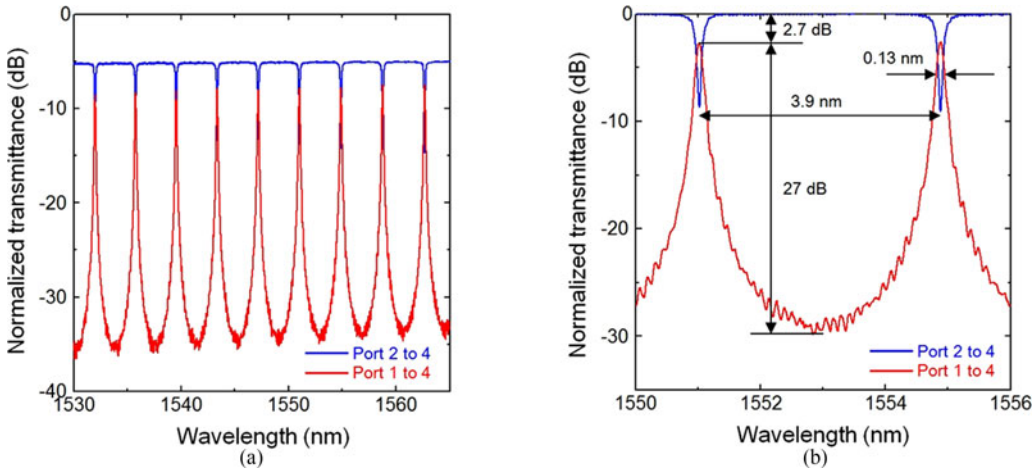

Fig. 3. Transmission spectrum, normalized by transmittance of (a) fiber-to-fiber and (b) reference SiN:D waveguide.

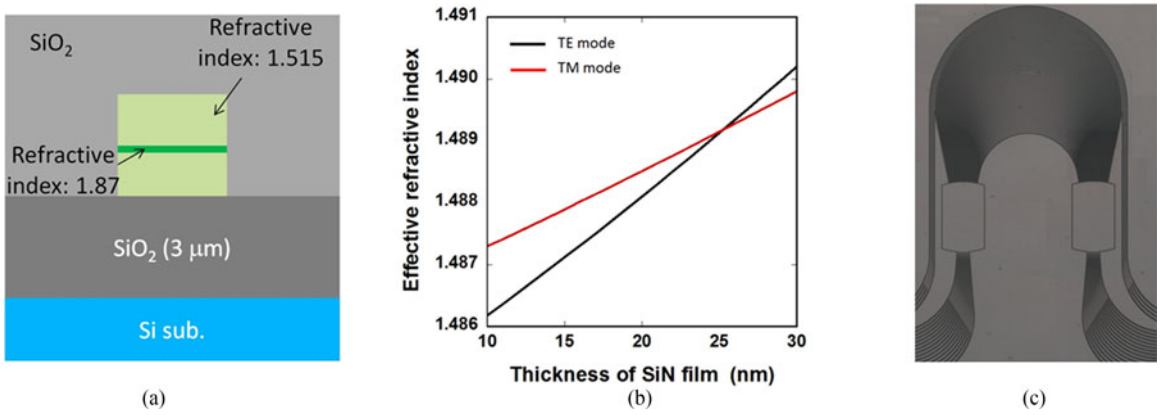

Fig. 4. (a) Schematic of SiON waveguide for polarization insensitivity. (b) Calculated relationships between effective refractive indices and thickness of SiN:D film. (c) Microscope image of fabricated AWG.

values are almost consistent with the calculated values. The 3-dB bandwidth was 0.13 nm and the extinction ratio was 27 dB in the entire C band.

3.2 Characteristics of Polarization-Insensitive AWG

We also used the SiON/SiN:D films to construct a polarization-insensitive AWG. The AWG was designed for 16 channels and a 200-GHz grid. Fig. 4(a) shows a schematic of the waveguide. We used a 3-μm-square core, which has enough allowable fabrication tolerance for lower crosstalk (<-25 dB) and polarization insensitivity. In this design the multi-layer core (SiON/SiN/SiON) compensated for the birefringence caused by the film stress [19]. Beforehand, we had already determined that the 3-μm-square SiON:D core with a refractive index of 1.515 has birefringence of $\sim 1.8 \times 10^{-3}$. Here, the birefringence was measured from the peak wavelength difference of the single-layer SiON-waveguide AWG between the transverse-magnetic (TM) mode and TE mode. Using the value, we calculated the required thickness of the SiN:D film (n = 1.87) to compensate for the birefringence. Fig. 4(b) shows the calculated relationships between effective refractive indices and thicknesses of the SiN:D film for TE and TM modes. The results show that we can compensate for the birefringence by using a 25-nm-thick SiN:D film for the core size of 3 μm^2.

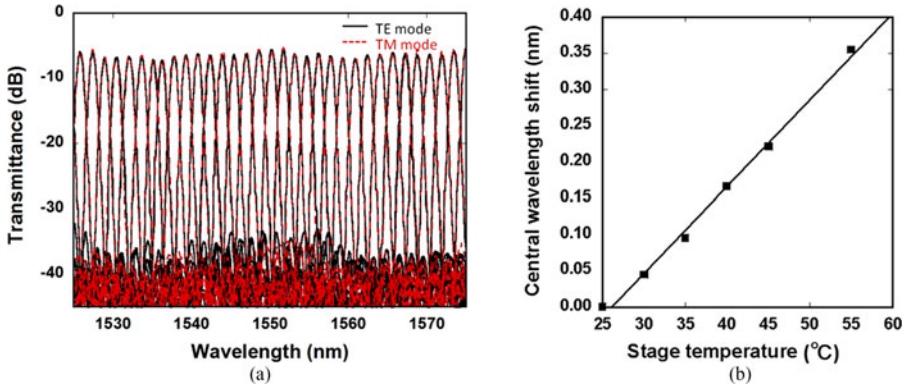

Fig. 5. (a) Transmission spectrum of fabricated AWG for TE- and TM-mode inputs, (b) relationship between central wavelength shift and temperatures.

In the fabrication process, the key feature is an in-situ and sequential deposition of multi-layer films (SiON/SiN/SiON) in the ECR CVD. To preciously control the thickness of both SiON and SiN films, we tuned the gas flow rate of SiD_4 and microwave power of the ECR plasma to obtain a moderate deposition rate ($\sim$100 nm/min), as shown in Fig. 1(a). The fabrication process was as follows. First, we deposited SiON/SiN/SiN films with refractive indices of 1.515 (SiON) and 1.87 (SiN) on the 3-μm-thick thermal-oxide of a Si substrate. Both the total multi-layer thickness (3 μm) and the SiN film thickness (25 nm) were preciously controlled by using the above deposition condition. The deposition temperature was around 200 degrees Celsius. Afterwards, the films were patterned by photolithography and the reactive-ion etching. Finally, a SiO_2 overcladding film of 6 μm was deposited at 300 degrees Celsius. All process temperatures were below 300 degrees Celsius and thus compatible with the BEOL-process temperature. Fig. 4(c) shows a microscope photograph of the fabricated multi-layer waveguide AWG.

We measured transmission specrum of the fabricated AWG. Although the AWG has 16 $\times$ 16 ports, we used one central input port and 16 output ports for the measurements. In the experimental setup, an amplified spontaneous emission light source in the C band was used. The input light was fed into a polarization controller and was then sent through a high numerical-aperture (NA) fiber, whose mode field diameter was around 4.3 μm. The mode field of the single-mode fiber was converted to that of the high-NA fiber through a thermally diffused expanded core (TEC) fiber. The high-NA fiber was cleaved and butt coupled to the facet of the AWG input port. The output ports of the AWG were also coupled to the high-NA fiber, which was connected to the optical spectrum analyzer. Fig. 5(a) shows the transmission spectrum of the AWG chip for TE- and TM-mode inputs. The transmittance was normalized by the fiber-to-fiber transmittance. The total insertion loss for TE and TM modes, including the two fiber-coupling facets, were 5.6 and 5.3 dB at the center port, respectively. Here, the propagation loss of the SiON:D waveguide was 0.29 dB/cm at 1550 nm. The interchannel crosstalk was less than $-$27 dB in the entire C band. Thanks to the low-loss SiON:D waveguide, the spectrum was not degraded at wavelengths near 1500 nm. In addition, the polarization dependence of the AWG was less than 0.1 nm. The precious control of the refractive-indices and the film thickness enabled us to compensate for the birefringence as designed. We also measured the central wavelength shift while changing stage temperature. Fig. 5(b) shows the measured results. In the experiment, the input mode was the TE mode and the central wavelength was around 1547 nm. The wavelength shift, estimated form the linear approximation, was 0.012 nm/K. The value is comparable to that of a conventional silica-based AWG. Although the thermo-optic coefficient of the SiN:D film was larger ($\sim 4 \times 10^{-5}$ /K) than that of the silica, the temperature dependence was only slightly degraded because the SiN:D thickness to compensate for the birefringence is very small. These results indicate the SiN:D/SiON:D waveguide system enables a low-loss, low-crosstalk, polarization-insensitive, and low-thermo-optic-effect wavelength filter on the Si photonic platform.

4. Conclusion

We fabricated the low-loss SiN/SiON waveguides at a CMOS backend process temperature. A hydrogen-free gas source was used to avoid N-H bond formation during the ECR CVD process. A fabricated SiN waveguide with delta of ∼20% showed propagation loss of less than 0.55 dB/cm in the entire C band. A ring resonator constructed with the waveguide showed a 3-dB bandwidth of 0.13 nm and an extinction ratio of 27 dB. In additions, a SiON waveguide whose delta was ∼3% showed propagation loss of 0.29 dB/cm. A 200-GHz AWG with multi-layer core of SiON/SiN/SiON showed insertion loss of less than 5.6 dB, crosstalk of less than −27 dB, and polarization-dependent peak-wavelength shift of less than 0.1 nm. With the large fabrication tolerance and the low optical loss, the hydrogen-free SiN/SiON waveguide is a promising component to construct high-performance C-band WDM filters for the next generation WDM optical network.

Acknowledgment

The part of research results have been achieved by “R&D on optical PLL device for receiving and monitoring optical signals,” Commissioned Research of National Institute of Information and Communications Technology, Japan.

References

[1] M. Paniccia, “Integrating silicon photonics,” *Nature Photon.*, vol. 4, pp. 498–499, 2010.
[2] F. G. D. Corte, S. Rao, G. Coppola, and C. Summonte, “Electro-optical modulation at 1550 nm in an as-deposited hydrogenated amorphous silicon p-i-n waveguiding device,” *Opt. Exp.*, vol. 19, pp. 2941–2951, 2011.
[3] J. F. Liu *et al.*, “Waveguide-integrated Ge p-i-n photodetectors on SOI platform,” presented at the IEEE Int. Conf. Group IV Photon., Ottawa, ON, Canada, 2006, Paper ThA2.
[4] D. Ahn *et al.*, “High performance, waveguide integrated Ge photodetectors,” *Opt. Exp.*, vol. 15, pp. 3916–3921, 2007.
[5] Y.-H. Lin and S.-L. Tsao, “Improved design of a 64 × 64 arrayed waveguide grating based on silicon-on-insulator substrate,” *IEE Proc., Optoelectron.*, vol. 153, pp. 57–62, 2006.
[6] W. Bogaerts *et al.*, “Compact wavelength-selective functions in silicon-on-insulator photonic wires,” *IEEE J. Sel. Topics Quantum Electron.*, vol. 12, no. 6, pp. 1394–1401, Nov./Dec. 2006.
[7] J.-X. Cain *et al.*, “Transmission of 96×100G pre-filtered PDM-RZ-QPSK channels with 300% spectral efficiency over 10,608 km and 400% spectral efficiency over 4,368 km,” presented at the Opt. Fiber Commun. Conf., San Diego, CA, USA, 2010, Paper PDPB10.
[8] J. Li, E. Tipsuwannakul, T. Eriksson, M. Karlsson, and P. A. Andrekson, “Approaching Nyquist limit in WDM systems by low-complexity receiver-side duobinary shaping,” *J. Lightw. Technol.*, vol. 30, no. 1, pp. 1664–1676, Jun. 2012.
[9] J. Zhao and A. D. Ellis, “A novel optical fast OFDM with reduced channel spacing equal to half of the symbol rate per carrier,” presented at the Opt. Fiber Commun. Conf., San Diego, CA, USA, 2010, Paper OMR1.
[10] K. Okamoto, “Progress and technical challenge for planar waveguide devices: silica and silicon waveguides,” *Laser Photon. Rev.*, vol. 6, pp. 14–23, 2012.
[11] K. Yamada, “Back-end photonics for silicon-based integrated photonic platform,” presented at the Asia Commun. Photon. Conf., Hong Kong, 2015, Paper ASu3A.4.
[12] H. Fukuda *et al.*, “Four-wave mixing in silicon wire waveguides,” *Opt. Exp.*, vol. 13, pp. 4629–4637, 2005.
[13] Z. Zhang *et al.*, “A new material platform of Si photonics for implementing architecture of dense wavelength division multiplexing on Si bulk wafer,” *Sci. Technol. Adv. Mater.*, vol. 18, pp. 283–293, 2017.
[14] S. C. Mao *et al.*, “Low propagation loss SiN optical waveguide prepared by optimal low-hydrogen module,” *Opt. Exp.*, vol. 16, pp. 20809–20816, 2008.
[15] C. R. Doerr, L. Chen, L. L. Buhl, and Y. K. Chen, “Eight-channel SiO2/Si3N4/Si/Ge CWDM receiver,” *IEEE Photon. Technol. Lett.*, vol. 23, no. 17, pp. 1201–1203, Sep. 2011.
[16] L. Chen, C. R. Doerr, L. Buhl, Y. Baeyens, and R. A. Aroca, “Monolithically integrated 40-wavelength demultiplexer and photodetector array on silicon,” *IEEE Photon. Technol. Lett.*, vol. 23, no. 13, pp. 869–871, Jul. 2011.
[17] T. Barwicz, M. A. Popović, M. R. Watts, P. T. Rakich, E. P. Ippen, and H. I. Smith, “Fabrication of adddrop filters based on frequency-matched microring resonators,” *J. Lightw. Technol.*, vol. 24, no. 5, pp. 2207–2218, May 2006.
[18] M. J. Shaw, J. Guo, G. A. Vawter, S. Habermehl, and C. T. Sullivan, “Fabrication techniques for low-loss silicon nitride waveguides,” *Proc. SPIE*, vol. 5720, pp. 109–118, 2005.
[19] H. Nishi *et al.*, “Low-polarization-dependent silica waveguide monolithically integrated on SOI photonic platform,” *J. Lightw. Technol.*, vol. 31, no. 11, pp. 1821–1827, Jun. 2013.
[20] K. Okazaki et al., “Optical coupling between SiO_xN_y waveguide and Ge mesa structures for bulk-Si photonics platform,” presented at the IEEE Int. Conf. Group IV Photon., Vancouver, BC, Canada, 2015, Paper WP43.
[21] T. Tsuchizawa *et al.*, “Monolithic integration of silicon-, germanium-, and silica-based optical devices for telecommunications applications,” *IEEE J. Sel. Topics Quantum Electron.*, vol. 17, no. 3, pp. 516–525, May/Jun. 2011.
[22] T Hiraki *et al.*, “Si-Ge-silica monolithic integration platform and its application to a 22-Gb/s × 16-ch WDM receiver,” *IEEE Photon. J.*, vol. 5, no. 4, Aug. 2013, Art. no. 4500407.